AIAA JOURNAL
Vol. 40, No. 3, March 2002

Two-Dimensional Synthetic Jet Simulation

Conrad Y. Lee* and David B. Goldstein†
University of Texas at Austin, Austin, Texas 78712-1085

Direct numerical simulation was used to model an array of two-dimensional synthetic slot jets pulsing into initially quiescent flow. Such zero-net mass-flux jets can represent an array of microelectromechanical systems. Fluid ejected by the pulsing jets rolls up into vortex pairs that propagate as a result of their mutually induced velocity and the initial momentum given by the pulse. The effects of fluid and geometric parameters on the resulting flowfield were studied. The results near the slots were compared with experimental data and found to be in good agreement.

Nomenclature

A	=	maximum piston velocity
AR	=	area ratio between piston and slot, h_{piston}/h
F_s	=	body force applied at a boundary point
f	=	frequency of piston motion
h	=	slot width
h_{piston}	=	piston width
$h_{1/2}$	=	slot half-width
I_0	=	average impulse per unit width
L_0	=	stroke length
Re	=	device Reynolds number, $U_{\text{peak}}h_{1/2}/\nu$
Re_{I_0}	=	Reynolds number based on average impulse, $I_0/\mu h_{\text{jet}}$
Sr	=	device Strouhal number, $2\pi f h_{1/2}/U_{\text{peak}}$
T	=	period of oscillation
U_{desired}	=	desired velocity of a boundary point
U_{peak}	=	maximum average jet velocity across the slot, $AR \times A$
U_{piston}	=	piston velocity, $A\sin(2\pi f)$
U_s	=	actual velocity of a boundary point
U_0	=	average jet velocity, L_0/T
u, v	=	flow velocities
$u_0(t)$	=	instantaneous mean jet velocity at the slot plane
x_s	=	coordinates of boundary points
α	=	gain of force field
β	=	damping of force field
ΔU_s	=	difference between local and desired velocity, $U_s - U_{\text{desired}}$
ν	=	dynamic viscosity
Ω	=	vorticity

I. Introduction

RECENT advances in micromachining techniques have allowed the construction and testing of low-power microelectronic mechanical systems (MEMS) devices for flow control such as flaps, surface heating elements, and synthetic jets. Synthetic jets are of particular interest as sturdy active control devices of zero-net mass flux requiring no internal fluid supply lines. Some applications for such devices include improving heat transfer, jet vectoring, enhancing mixing, and controlling a turbulent boundary layer for drag reduction. Slot jets constructed by Smith and Glezer[1] consist of a small cavity enclosed on one side by a membrane driven by a piezoelectric actuator and on the other side by a surface containing a high-aspect-ratio aperture (Fig. 1). Other experimental studies of the flow generated by synthetic jets have been performed,[2,3] but, to date, there have been only a few detailed simulations seeking to better understand the physics of the flow.

Kral et al.[4] solved a boundary-value problem for the incompressible, unsteady two-dimensional Reynolds-averaged Navier–Stokes equations with the Spalart–Allmaras turbulence model. The computational domain encompassed only the region external to the jet without the cavity or actuating membrane. The jet presence was simulated by forcing an analytical velocity profile on the boundary region corresponding to the jet orifice. Results appeared to agree with the the experimental observations by Smith and Glezer[1]: the near flowfield is dominated by the formation of counter-rotating vortex pairs. Further away from the jet aperture, the vortex cores become smeared by turbulent diffusion. In the experiments the vortices break down into a planar turbulent jet beyond approximately 8–10 slot widths of the aperture.

Rizzetta et al.[5] used direct numerical simulation (DNS) to solve the unsteady, compressible Navier–Stokes equations. The external region, the cavity itself, and the throat were calculated on separate grids and linked through a chimera methodology. The membrane motion was represented by varying the position of appropriate boundary points. In addition to confirming the findings of Kral et al.,[4] Rizzetta et al.[5] showed that the internal cavity flow becomes periodic after several cycles. Therefore, it was considered appropriate to sample and use the periodic velocity profile at the slit plane as a boundary condition in subsequent runs involving the external domain only. Three-dimensional simulations indicate that the external flow breakdown into a turbulent jet observed in experiments was a result of three-dimensional instabilities, which also explained why no such phenomena were observed in any strictly two-dimensional simulations. The same conclusion was reached by Mallinson et al.[6] when comparing experiments and simulations of round jets.

The computational studies, in tandem with experiments, provide useful knowledge about the physics of the flow. However, there are still a wide range of geometric and flow parameters left to examine. Moreover, the issue of coupling the available simulations to the turbulent flow to be controlled has not been fully addressed. Thus, an alternate method, which is relatively simple to implement and does not require excessive computer resources, is presented. Such simulations can find applications in the design of synthetic jets in general and as complement to experiments. The method we use has already been proven by Goldstein et al.[7] and Goldstein and Tuan[8] as adequate for DNS simulation of turbulent boundary layers. For turbulent boundary-layer control, even though boundary-layer Reynolds numbers are large, the actuators are to be used to control flow structures in the buffer layer. Hence, the MEMS are expected to operate at a very low local Reynolds number, $Re \approx \mathcal{O}(10)$. Experiments by Breuer et al.[9] showed that slot jets operating in such a range can cause local reductions in shear stress, whereas numerical work[10] has demonstrated that flow generated by such low-Reynolds-number pulsed jets can affect coherent structures well beyond the buffer layer. The present simulations are carried out so that, assuming they

Received 6 April 2000; revision received 7 April 2001; accepted for publication 5 September 2001.

*Graduate Research Assistant, Center for Aeromechanics Research, Department of Aerospace Engineering and Engineering Mechanics. Student Member AIAA.

†Associate Professor, Center for Aeromechanics Research, Department of Aerospace Engineering and Engineering Mechanics. Senior Member AIAA.

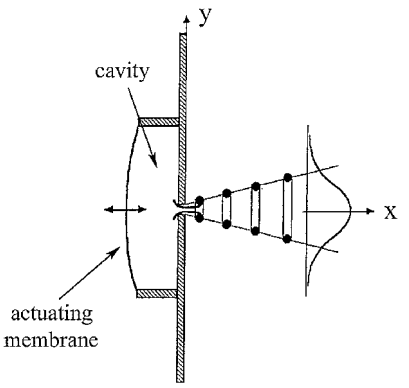

Fig. 1 Schematic of synthetic jet (from Ref. 1).

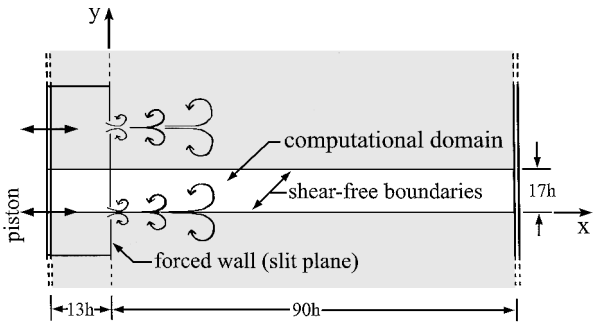

Fig. 2 Schematic of periodic array of pulsing jets and computational domain.

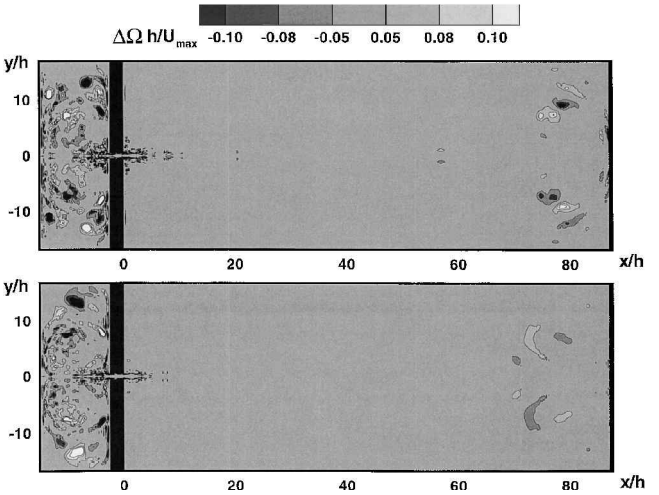

Fig. 3 Contours of normalized vorticity difference between grid sizes (top = 512 × 256 and 512 × 512, bottom = 512 × 512 and 512 × 1024) at $Re = 416.6$.

can be validated, the same computational procedures will remain valid when coupled with a DNS of a turbulent boundary layer.

The computational approach is briefly described in Sec. II. A study on the correctness of the method is described (Sec. III.A.), and further simulations examine several flow and geometric parameters (Secs. III.B and III.C). Throughout this study results are compared to earlier numerical studies and experiments.

II. Numerical Procedure

The DNS method used in this simulation is based on that developed by Kim et al.[11] to examine turbulent channel flow. The Navier–Stokes equations are manipulated to give a fourth-order system of equations for the spanwise v component of velocity. The equations are solved with a Chebyshev-tau method with grid clustering near the edges of the domain. Time stepping is done with an Adams–Bashforth/Crank–Nicholson scheme. Once v is known, the streamwise u is obtained from the continuity equation in spectral space and projected back onto physical space. Spectral representations make this method attractive because of the low computational cost of fast transform methods and for the accuracy of results.

Modifications made to the code allow the use of virtual surfaces to define both the solid and moving walls. This method, related to that of Peskin[12] and developed by Goldstein et al.,[7,13] imposes a localized body force along desired points in the computational mesh to bring the fluid there to a specified velocity so that the force has the same effect as a solid boundary. The desired velocity is incorporated in a iterative feedback loop to determine the appropriate force. For example, given a moving boundary with velocity $U_{\text{desired}}(x_s, t)$, an expression for the body force F_s is

$$F_s(x_s, t) = \alpha \int_0^t (\Delta U_s)\, \mathrm{d}t' + \beta(\Delta U_s) \tag{1}$$

The constants α and β are negative and defined as the gain and damping of the force field with dimensions of $M/(L^3T^2)$ and $M/(L^3T)$, respectively. This approach allows for fairly complex geometries and/or moving boundaries to be incorporated in a regular domain without the usual complexities of mapping. Previous studies by Goldstein et al.[7] confirmed the success of this technique for modeling a riblet surface below a turbulent boundary layer with only a 5% increase in computational time when compared to conventional boundary definitions of a solid flat surface.

III. Results

A. Flow Parameters

A schematic of an array of actuators and the computational domain is shown in Fig. 2. The moving piston and the solid wall separating the internal from the external flow are defined with the virtual surface method. The left and right domain boundaries are periodic, and the top and bottom walls are defined as shear-free boundaries. As highlighted in Fig. 2, the computational domain corresponds to half of the actual physical domain. In this study the flow parameters of importance are the device Reynolds number Re and Strouhal number Sr defined according to U_{peak} and $h_{1/2}$. The piston motion is emulated by imposing a sinusoidal velocity U_{piston} within a few columns of boundary cells defining the piston. For an incompressible fluid the mean jet velocity at the orifice at any instant $u_0(t)$ and the maximum average jet velocity U_{peak} can then be determined simply from the area ratio between the piston and jet aperture. Also of interest are the stroke length L_0 and the average impulse per unit width I_0 given as

$$L_0 = \int_0^{T/2} u_0(t)\, \mathrm{d}t \qquad I_0 = \rho h \int_0^T u_0^2(t)\, \mathrm{d}t \tag{2}$$

From the definitions of $u_0(t)$ and U_{peak}, it can be shown that for this study Sr is exactly h/L_0. The preceding also allows us to define an average jet velocity U_0 and the Reynolds number based on average impulse Re_{I_0}.

B. Quality of the Solutions

We first describe a single simulation at $Re = 416.6$ and $Sr = 0.0628$ used for checking grid convergence. As already mentioned, the computational domain is half the actual domain, and the baseline grid contains 512 cells in the streamwise x direction and 128 in the spanwise y direction. The forced wall separating internal and external flow was defined as a single column of forced grid points, whereas the piston surface was defined over three columns of grid points, which yields effective thicknesses of 0.2 and $0.6h$, respectively. Throughout this paper the force-field parameters were $\alpha = -500{,}000$ and $\beta = -300$. Grid independence is verified by using the difference between time-averaged vorticity fields for increasing grid sizes as an indication of the convergence of the solution. For all grid sizes data were taken over the last five cycles of a 20-cycle run. Because the domain is shown with its mirror image, the baseline grid in the figure has in reality 512 × 256 cells, whereas the finer grids have 512 × 512 and 512 × 1024 cells. For the Reynolds number of 416.6, Fig. 3 shows considerable noise in the cavity and the right-hand side of the domain. As explained later, the flows at

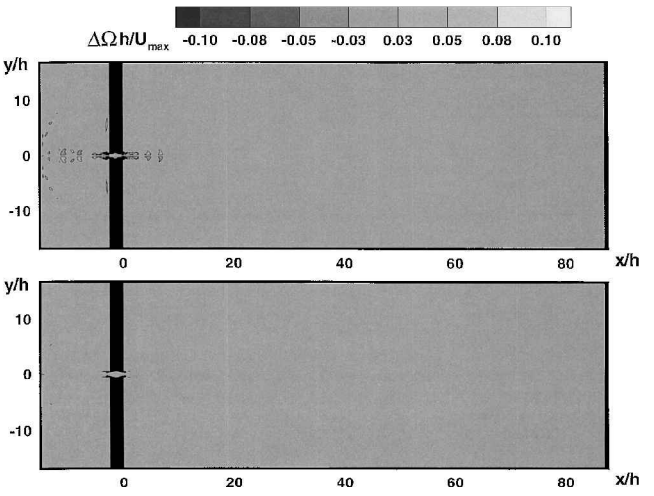

Fig. 4 Contours of normalized vorticity difference between grid sizes (top = 512 × 256 and 512 × 512, bottom = 512 × 512 and 512 × 1024) at $Re = 104.2$.

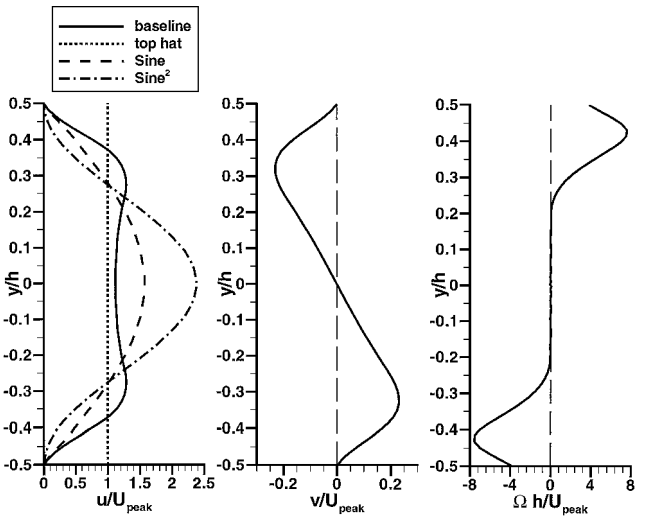

Fig. 5 Flow velocities and vorticity for baseline case ($Re = 104.2$, $Sr = 0.0628$) and comparison to analytical expressions at peak blowing.

these locations and at this high Reynolds number are fairly chaotic, which causes the discrepancy. However, between the two chaotic regions, there is a broadband from $x/h = 0$ to $x/h \approx 60$, where the flow is nearly periodic in time and the vorticity difference between grids is minimal to nonexistent. Because data used to compare the simulation to the experiments were taken from $0 \leq x/h \leq 40$, it is reasonable to assume the solution is grid independent in this region of interest. An identical study was performed for the lower Reynolds number of 104.2, at which the geometric parameters' study was performed. Results are shown in Fig. 4, and because stable periodic cells formed at both ends of the domain, the differences between grids are minimal throughout the entire domain. Therefore, at the lower Reynolds number it is safe to assume that the baseline grid (512×128) is converged over the entire domain. Throughout the study time accuracy was maintained by adjusting the time step so that each period of actuation corresponded to at least 3000 time steps and by monitoring the Courant–Friedrichs–Lewy number.

As noted in the preceding section, the current simulation is limited to two-dimensional. Experimental results indicate that the vortices formed become unstable and breakdown into a turbulent jet within $x/h = 10$ of the slot. However, comparison to experiments covered in Sec. III.F indicate that there is a fair agreement between the data presented here and experiments for a region $x/h \leq 8$. Consequently, the current results are still valuable in giving insight to the near-field jet behavior and its susceptibility to flow and geometric effects.

C. Baseline Case

Smith and Glezer[1] performed experiments at Reynolds and a Strouhal numbers of 416.6 and 0.0628, respectively, but our simulations at those parameters produce a rather complex flowfield. To better isolate the effect of a single geometric or flow parameter, a baseline case was selected by running the code on the baseline grid at a lower $Re = 104.2$ with a simpler flow field. The $Re = 416.6$ case will be examined in Secs. III.D. and III.F.

As already mentioned, Kral et al.[4] made use of analytical expressions for the streamwise u velocity while the spanwise v velocity was taken as zero at the slit plane. Figure 5 contains plots of instantaneous streamwise u velocity, spanwise v velocity, and vorticity Ω in the slit plane at the moment of peak blowing. Also plotted for the case of the u velocity are the analytical expressions used by Kral et al.[4] As seen in the figure, u is "horned" at the edges with peaks around $y = \pm 0.3h$ and does not resemble a parabola or the other profiles shown. This deformation conforms to the profile distortions common to oscillatory flows as the low-momentum boundary layer accelerates more quickly than the bulk flow. Moreover, the spanwise v is clearly nonzero and has variations as high as $\pm 0.24 U_{\text{peak}}$, whereas the vorticity peaks at $y = \pm 0.41h$. The simulation results reflect the use of a single column of grid cells to define the solid

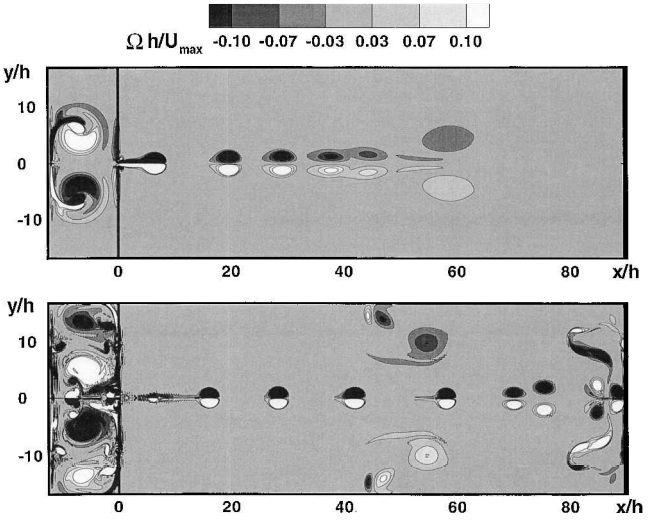

Fig. 6 Vorticity contours for different Reynolds numbers (top: baseline case of $Re = 104.2$, $Sr = 0.0628$; bottom: $Re = 416.6$, $Sr = 0.0628$).

walls and jet orifice. Such a near infinitely thin wall promotes flow separation and does not allow a significant boundary layer to develop within the throat. Consequently the u velocity profile is far from parabolic, and there is a substantial velocity component in the spanwise y direction.

A vorticity contour plot of the baseline case after 10.5 cycles is shown at the top of Fig. 6. The external flow to the right of the slit plane presents a phenomena not noted in previous numerical simulations: continuous vortex pairing of the leading vortices. Vortex pairing was not observed either in the experiments by Smith and Glezer[1] perhaps because the vortices break down into turbulence within several h of the jet aperture. Pairing in the present simulation is believed to be a consequence of the closed periodic domain of the simulation: leading vortices face a counterflow caused by the far wall and consequently slow down, allowing subsequent vortices to catch up to their position. The flow eventually reaches a steady-state condition in which vortices formed by ejected fluid diffuse and become too smeared for any pairing event to be observed. The internal cavity or plenum flow is also seen. As found by Rizzetta et al.,[5] a single main circulation cell develops after only a few cycles. The circulation cell grows and seems to reach a quasi-steady state after about 25 cycles.

D. Reynolds and Strouhal Numbers Study

The effects of the flow parameters Re and Sr were examined by independently varying them about the baseline case.

Reynolds-number dependence was examined by maintaining $Sr = 0.0628$ while increasing or decreasing the Reynolds number by factors of 4–26.38 and 416.6 through variations of the kinematic viscosity. At very low $Re = 26.38$ the vortices formed by ejected fluid dissipate within $20h$ of the aperture without pairing. However, increasing to $Re = 416.6$ allows the ejected vortices to remain coherent long enough to impact against the far right wall (Fig. 6) and flow back toward the slit. The backflowing vortices remain coherent enough to affect the translational speed (celerity) of centerline pairs. Pairing events were also observed between individual centerline vortices, but no discernible pairing pattern was observed as a result of the complex flow associated with all of the vortical structures in the domain.

Flow within the cavity at the low $Re = 26.38$ does not form a circulation cell as vorticity quickly dissipates. However, at $Re = 416.6$ complex activity can be seen within the cavity, which does not reach stable periodicity even after the longest run of 37 cycles. Eddies impacting against the piston in the plenum produce vorticity, which is scooped from the solid walls. Those secondary vortices do not dissipate quickly and thus continuously add to the complicated picture.

The effect of Reynolds-number variation on the jet properties across the slit are shown on the left of Fig. 7. The u profile at a low Reynolds number looses the edge horns, and the profile looks like a flattened parabola, whereas for a higher Reynolds number the horns are more pronounced. This effect can be traced to the behavior of oscillatory boundary layers that form in the throat region. As noted in Schlichting,[14] an oscillatory boundary layer grows proportionaly to $(\nu/\omega)^{1/2}$ so that the horns at higher Reynolds numbers are the result of thinner boundary layers in the throat. Although not shown, the vertical velocity profile has a slight decrease in magnitude, and the location of peak v moves towards the centerline as the Reynolds number decrease. A similar but less pronounced trend was observed in the peak vorticity across the slit.

Strouhal-number dependency was examined by holding the Reynolds number fixed at 104.2 while varying Sr by factors of 4–0.0157 and 0.2512 through changes in frequency. Because of the equivalent relation between Sr and h/L_0, there is an inversely proportional change in the normalized stroke length as well. Comparisons of the u velocity at the jet plane for different Sr on the right of Fig. 7 show that the overall shape of the u profile at the slit remains unchanged. There is only a slight tendency to increase the magnitude of u as Sr decreases. Similar small variations are observed in the v velocity while the vorticity remains mostly unchanged.

Effects on vorticity are shown in the contour plots of Fig. 8 and reflect the changes to L_0. As seen in the top figure, for a high-Strouhal-number case a much smaller amount of fluid is ejected by the reduced L_0 per half-pulse. Consequently, the ejected vortices continually merge within $\mathcal{O}(1h)$ of the jet aperture into a pair of vortex sheets. The vortex sheets dissipate quickly but still maintain a faint jet head even out to $x \approx 40h$ after 40 cycles. The low-Strouhal-number case on the bottom figure presents the opposite physical effect: the long stroke causes large amounts of fluid to be ejected. As a result, the vortex pairs are spaced far apart so that there is no pairing.

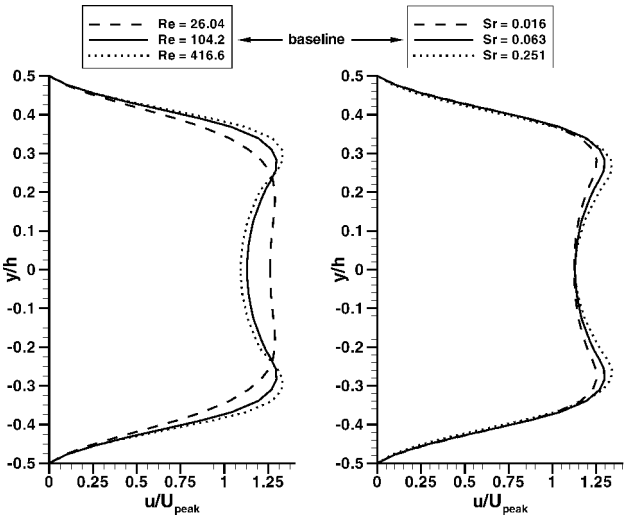

Fig. 7 Comparison of peak streamwise velocity for baseline case and different flow parameters at peak blowing.

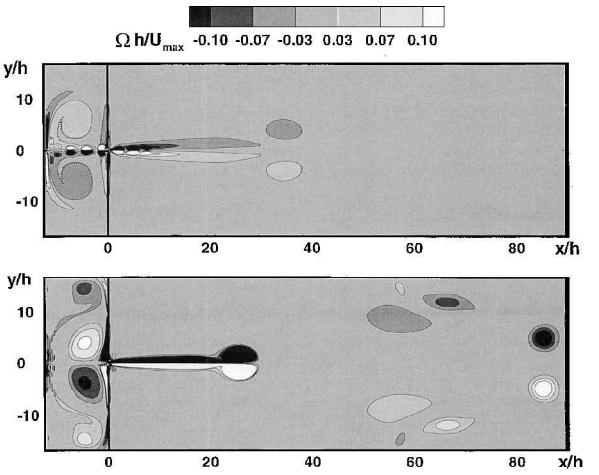

Fig. 8 Vorticity contours for different Strouhal numbers (top: baseline case of $Re = 104.2$, $Sr = 0.2512$; bottom: $Re = 104.2$, $Sr = 0.0016$).

Internal to the plenum chamber, the high Strouhal number produces a faint circulation cell (Fig. 8, top). The low-Strouhal-number case establishes a circulation cell that, unlike the baseline case, moves in a rough circular orbit and distorts according to the piston motion (Fig. 8, bottom). As the circulation cell moves about the plenum, extra vorticity is shed by boundaries forming weak secondary circulation cells near the top and bottom of the cavity.

E. Geometric Parameters Study

Although the flow parameters of interest are mainly the Reynolds and Strouhal numbers, there are many geometric parameters that can be varied in such a device. In this section the effects of the lip thickness and shape and the domain length (both external and internal) on the flow are examined. All studies are performed on the baseline grid of 512×128 at $Re = 104.2$ and $Sr = 0.0628$.

Lip Thickness

For the baseline case the wall separating the internal and external domains was defined by a single column of gridpoints. Although there was no leakage observed across the wall, the corresponding physical condition would be of a sharp plate of near-zero thickness. Consequently, a parametric study on the effects of lip thickness was performed by progressively adding layers to the plate until the dividing wall and the lip were $2.5h$ thick. Figure 9 shows the effect of thickening the wall on the u velocity at the outer slit plane. Compared to the baseline case, the horns of the profile disappear for a $1h$-thick wall, and the profile is insensitive to walls thicker than $2h$. Thicker walls allow a boundary layer to develop within the slit but not to the extent that it becomes fully developed as in pipe flow. Rather the effect is similar to an entry region of a pipe, and the overall effect of the boundary layers is to reduce the actual throat height at the exit plane. This increases the peak streamwise velocity, but, because the flow still separates at the sharp corner edge of the lip, there is little change in the v velocity or vorticity.

In the external flow the thicker lip causes an increase in the celerity of the ejected vortices caused by the development of thicker boundary layers. This increased celerity is seen in the contour plot of Fig. 9. In the figure baseline case vorticity contours are shown in gray scale while the $2h$-thick lip case is drawn in lines after four cycles. The internal cavity flow was similarly affected as the increase in celerity causes the vortices of the thicker lip to impact earlier in the cycle against the piston face. As a result, the circulation cell created is slightly out of phase compared to the baseline case. There is no change, however, in the period or size of the circulation cell

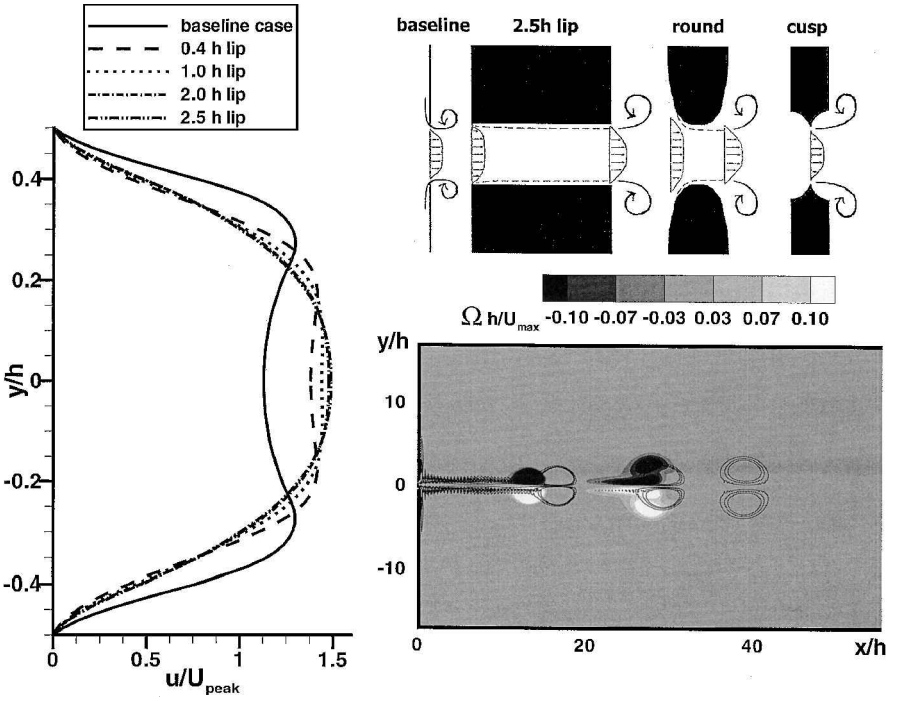

Fig. 9 Schematic of types of lips used and effect of thickening lips on streamwise velocity at peak blowing and vorticity contours.

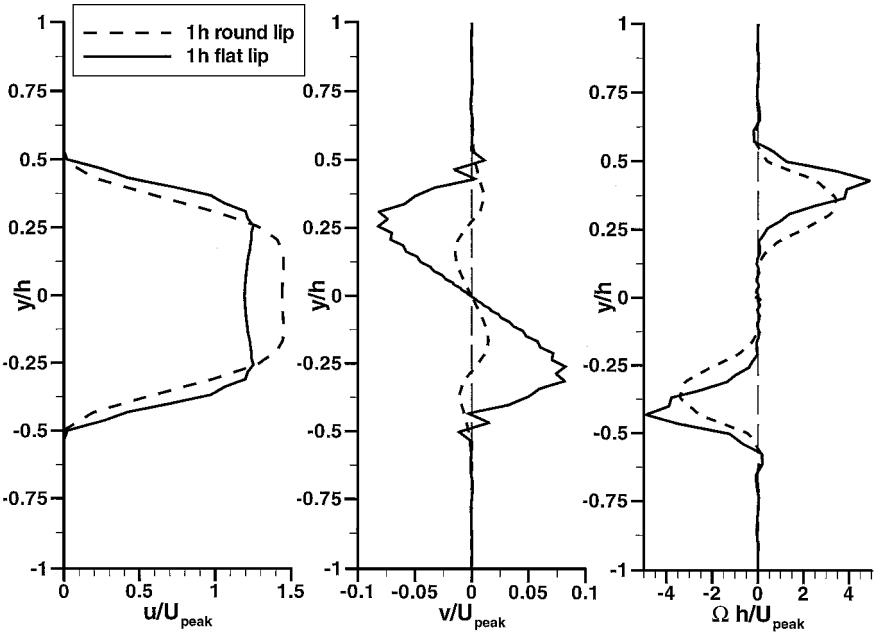

Fig. 10 Comparison effects of round and flat lips on flow properties at peak blowing.

because those parameters are set by the period of oscillation of the piston and cavity depth.

Lip Geometry

To examine the effect of the lip geometry on the flow, two other types of lips are used: a sharp, cusp-shaped lip and a smoothed, rounded lip as shown schematically on the top of Fig. 9. Flow properties at the center of the slit cross plane are shown in Fig. 10 for the rounded lip and flat lips. When compared to the flat lip, the rounded lip u profile shows approximately a 20% peak reduction. The round-lip v profile is increased by a factor of four, and peak vorticity Ω is increased by 40%. This result is not entirely surprising: the smooth shape of the lip inhibits entrance separation and forms a vena contracta through the slot. Close-up examination of the flow around the throat shows that the rounded lip allows more fluid to be entrained from the sides during a suction phase, causing the increase in the spanwise velocity. For the cusped lip a similar increase in the u velocity is observed, but there is little variation in the v velocity and vorticity. Despite the variations in the u velocity, neither case substantially affected the celerity of the ejected vortices so that there were no substantial changes in the external or internal flows.

Size of Domain

Sensitivity of the flow to the size of the internal cavity is studied by halving the size of the internal cavity to $\frac{1}{2}$ and then to $\frac{1}{4}$ of the original baseline case. As the cavity becomes shallower, there is an increase in the celerity of the ejected vortices. Compared to the baseline case, the internal flow of the half-cavity case shows a smaller circulation cell, and as the simulation progresses part of the cell is pushed toward the slot in each blowing half-cycle. In contrast, the quarter-cavity case does not even form a circulation cell. Instead, all of the vorticity ingested in one half-cycle is fed back out through

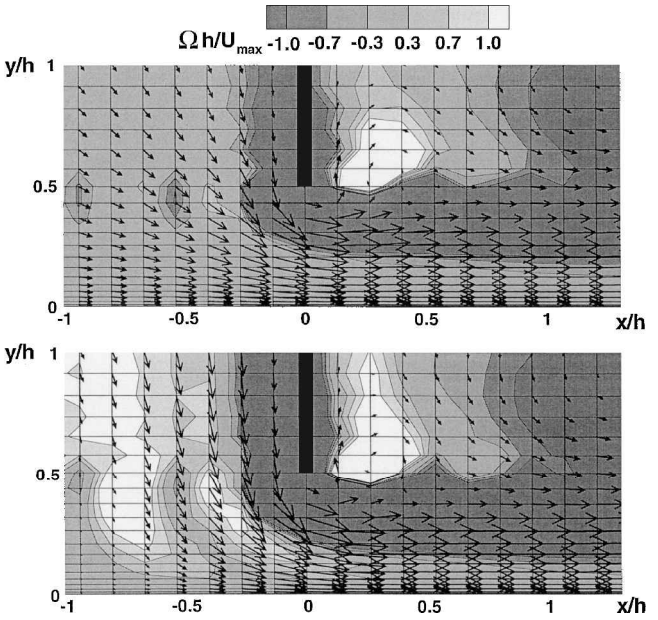

Fig. 11 Close-up of vorticity contours, vectors, and mesh around sharp lip orifice (top = baseline case, bottom = quarter-cavity case).

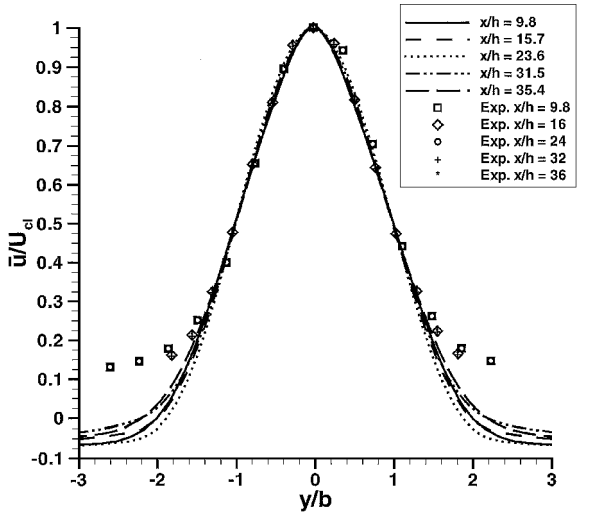

Fig. 12 Mean u velocity vs spanwise direction at different x/h streamwise distances from orifice for 2.5h-thick flat lips (Re = 416.6, Sr = 0.0628).

the slit during the following half-cycle. Figure 11 shows a close up of the flow around the lip for both the baseline and the quarter-cavity cases. In the quarter-cavity case positive vorticity is pushed closer to the dividing wall and the vorticity layer that forms the external jet. Because the positive cavity vorticity (clockwise in the figure) has opposite sign to the negative vorticity layer, it induces an increase in the vertical downward speed of the flow along the dividing wall as seen by the size and orientation of the vectors just inside the cavity. The overall effect of this added momentum is a slight effective narrowing of the slot width and an increase in the celerity of the ejected vortices.

F. Comparison to Experiments

The preceding flow and geometric parameter studies can be compared to experimental data of Smith and Glezer.[1] Those experiments were performed on a continuously running jet with 2.5h-thick flat lips at a Reynolds number of 416.6 and Strouhal number of 0.0628. Simulation data, in contrast, were accumulated over the last five cycles of a 35-cycle run. Figure 12 shows a plot of mean streamwise velocity $\bar{u}$ with respect to spanwise distance y from the centerline at several locations downstream of the jet slit. Also included are experimental data points at approximately the same locations. Normalization factors are the centerline velocity $\overline{U_{cl}}$ and the jet half-maximum width b. As seen in Fig. 12 and previous numerical studies, all data collapse well on a single curve showing that the similarity parameters for conventional jets also apply to oscillating jets. However, our mean u velocity becomes negative beyond a $y/b \approx \pm 2$. An explanation can be deduced from the time-averaged streamline plot of Fig. 13. Although the experiments were on a nearly isolated jet, the present study simulates the effect of an array of jets spaced 17h apart. The narrow, two-dimensional domain causes fluid feeding the centerline jet to be substantially drawn in from above and below so that a mean backflow is created outside of

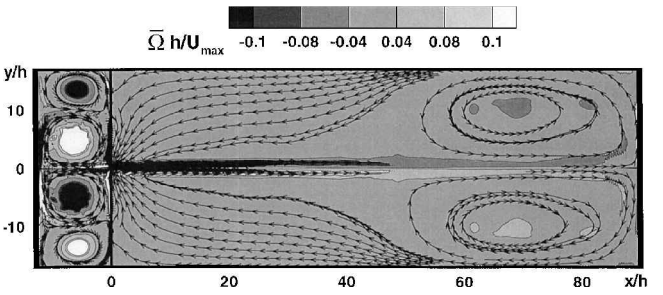

Fig. 13 Mean vorticity contours and streamlines after 35 cycles (Re = 416.6, Sr = 0.0628).

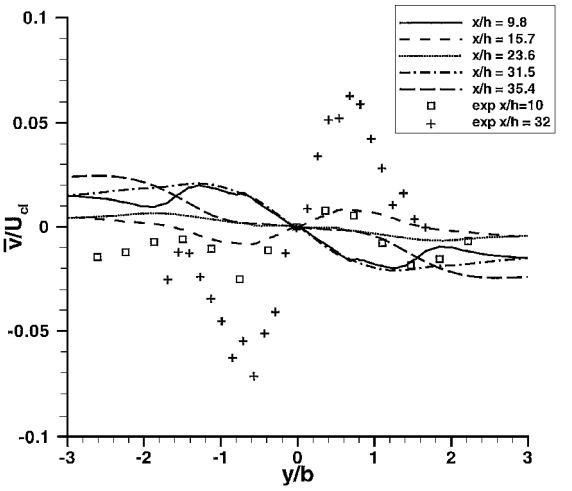

Fig. 14 Mean v velocity vs spanwise direction at different x/h streamwise distances from orifice for 2.5h-thick flat lips (Re = 416.6, Sr = 0.0628).

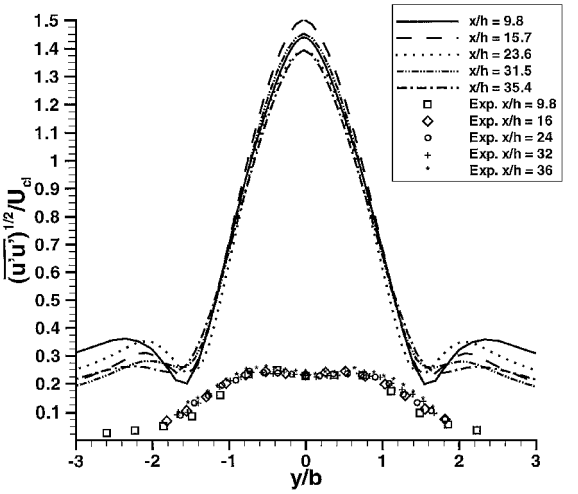

Fig. 15 Streamwise stress values vs spanwise direction at different x/h streamwise distances from orifice for 2.5h-thick flat lips (Re = 416.6, Sr = 0.0628).

the jet. Figure 14 shows the normalized mean spanwise velocity $\bar{v}$ plotted as in Fig. 12. Unlike $\bar{u}$, $\bar{v}$ does not match the experiment data in trend nor magnitude. Although the experiments indicate a $\bar{v}/U_{cl}$ variation of as much as 8%, the simulation data are contained in a narrowband of ±2.5%. This can be explained again by Fig. 13: the periodic nature of the simulation confines the jet to a narrow central band and limits the $\bar{v}$ variation. Figure 15 shows a plot of the autocorrelation of the u' velocity fluctuation. Data from the simulation show fluctuations $\mathcal{O}(10)$ times larger than the experimental values. This numerical result agrees with Rizzetta et al.[5] and is a consequence of the two-dimensional nature of the simulation, which does not model a breakdown into a three-dimensional turbulent jet.

Figure 16 shows the trajectory of a vortex blob starting at cycle 26 for both the thin sharp lip and the 2.5h-thick flat lip cases compared to experimental values. The x position is normalized by h and the time by period T. The computational and experimental vortex trajectories diverge far from the jet orifice but agree for a region $x/h < 8$, before the experimental breakdown into a turbulent jet. Figure 17 shows the centerline velocity normalized by U_0 against the position x/h. Again, there is fair agreement between the simulation and the experimental data for a region $x/h < 8$. This further confirms that although limited to such a small region the results from this simulation are comparable to experiments.

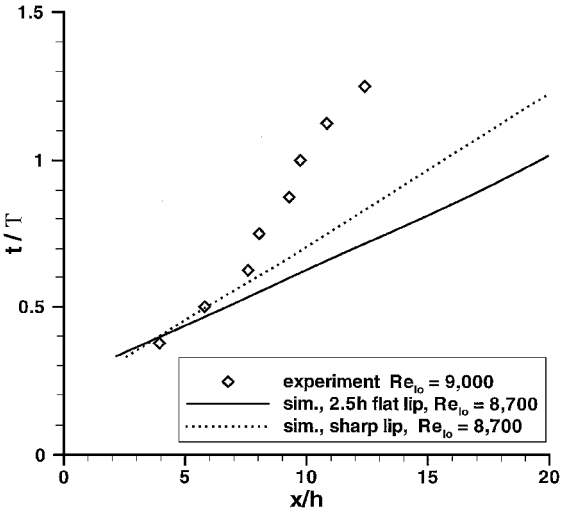

Fig. 16 Vortex trajectories from experiments compared to simulations. (Note greater celerity of 2.5h-thick flat lips.)

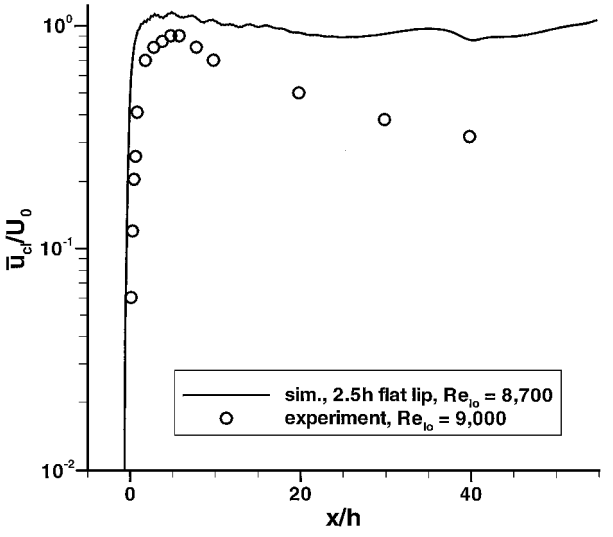

Fig. 17 Centerline velocity vs streamwise distance for experiments and simulation.

IV. Conclusions

An alternate direct numerical simulation method for simulating two-dimensional synthetic jets was presented. This method made use of the flexibility of virtual surfaces to examine in detail the physics of the resulting flow and its sensitivity to a host of flow and geometric parameters. Jet formation was observed to be highly sensitive to the flow Reynolds number, whereas jet evolution was affected by Strouhal number. In addition, the shape of the lip and depth of the cavity were also found to be important parameters in the resulting flow. Results were compared to experimental data and found to be in good agreement near the jet orifice. The results indicated the possibility of further applying this simulation method to study turbulent boundary-layer control because the local Reynolds number and geometric requirements would be much lower than the simulations presented here.

Acknowledgments

This work was supported by the U.S. Air Force Office of Scientific Research, Grant F49620-98-1-0027. We would like to acknowledge Ari Glezer and Barton Smith for their helpful conversations and sharing of data.

References

[1] Smith, B. L., and Glezer, A., "The Formation and Evolution of Synthetic Jets," *Physics of Fluids*, Vol. 10, No. 9, 1998, pp. 2281–2297.

[2] Smith, B. L., Trautman, M. A., and Glezer, A., "Controlled Interactions of Adjacent Synthetic Jets," AIAA Paper 99-0669, Jan. 1999.

[3] Smith, B. L., and Glezer, A., "Vectoring and Small-Scale Motions Effected by Free Shear Flows Using Synthetic Jet Actuators," AIAA Paper 97-0213, Jan. 1997.

[4] Kral, L. D., Donovan, J. F., Cain, A. B., and Cary, A. W., "Numerical Simulation of Synthetic Jet Actuators," AIAA Paper 97-1824, June 1997.

[5] Rizzetta, D. P., Visbal, M. R., and Stanek, M. J., "Numerical Investigation of Synthetic Jet Flowfields," *AIAA Journal*, Vol. 37, No. 8, 1999, pp. 919–927.

[6] Mallinson, S. G., Hong, G., and Reizes, J. A., "Some Characteristics of Synthetic Jets," AIAA Paper 99-3651, June 1999.

[7] Goldstein, D., Handler, H., and Sirovich, L., "Direct Numerical Simulation of Turbulent Flow over a Modeled Riblet Covered Surface," *Journal of Fluid Mechanics*, Vol. 302, 1995, pp. 333–376.

[8] Goldstein, D., and Tuan, T.-C., "Secondary Flow Induced by Riblets," *Journal of Fluid Mechanics*, Vol. 363, 1998, pp. 115–151.

[9] Breuer, K. S., Amonlirdviman, K., and Rathnasingham, R., "Adaptive Feed-Forward Control of Turbulent Boundary Layers," AIAA Paper 98-1025, Jan. 1998.

[10] Lee, C. Y., and Goldstein, D. B., "DNS of Microjets for Turbulent Boundary Layer Control," AIAA Paper 2001-1013, Jan. 2001.

[11] Kim, J., Moin, P., and Moser, R., "Turbulent Statistics in Fully Developed Channel Flow at Low Reynolds Number," *Journal of Fluid Mechanics*, Vol. 177, 1987, pp. 133–166.

[12] Peskin, C. S., "Flow Patterns Around Heart Valves: A Numerical Method," *Journal of Computational Physics*, Vol. 10, No. 2, 1972, pp. 252–271.

[13] Goldstein, D., Handler, H., and Sirovich, L., "Modeling a No-Slip Boundary with an External Force Field," *Journal of Computational Physics*, Vol. 105, No. 2, 1995, pp. 354–366.

[14] Schlichting, H., *Boundary-Layer Theory*, 7th ed., McGraw–Hill, New York, 1987, pp. 411–412.

P. Givi
Associate Editor